Electrochemical, Spectroscopic, and Theoretical Study of Trinuclear Ruthenacyclopentadienyl Clusters $Ru_3(\mu\text{-}CO)_2(CO)_6(RC_2R)_2$

Domenico Osella,* Giuseppina Arman, and Roberto Gobetto

Dipartimento di Chimica Inorganica, Chimica Fisica e Chimica dei Materiali, Università di Torino, Via P. Giuria 7, 10125 Torino, Italy

Franco Laschi and Piero Zanello*

Dipartimento di Chimica, Università di Siena, Siena, Italy

Simon Ayrton, Venetia Goodfellow, Catherine E. Housecroft,* and Steven M. Owen

University Chemical Laboratory, Cambridge, U.K.

Received January 10, 1989

The redox chemistry of triruthenium metallacyclopentadienyl clusters $Ru_3(CO)_8(RC_2R)_2$ has been investigated by electrochemical, spectroscopic, and theoretical techniques and compared with that of homologous triiron derivatives. The sequence of the electrode processes has been postulated on the basis of the responses of different electrochemical techniques, electron spin resonance (ESR) spectroscopy, and chemical tests. The linear correlations between the formal electrode potentials of these derivatives and the wavenumbers of the visible bands of their electronic spectra have been discussed on the basis of Fenske–Hall quantum mechanical approach carried out on the model compounds $M_3(CO)_8(HC_2H)_2$ (M = Fe, Ru) in the idealized C_{2v} geometry.

Introduction

The electrochemistry of organometallic clusters represents a recent aspect of their chemistry and may offer a clue for their efficient and selective electrosyntheses.[1]

In binary metal carbonyl clusters, the HOMO and LUMO are generally metal–metal bonding and antibonding in character, respectively. Thus the anodic oxidation and the cathodic reduction cause quick and irreversible cluster degradation. This is the case for $M_3(CO)_{12}$ (M = Ru, Os) series:[2]

$$M_3(CO)_{12} + 1e \rightleftarrows [M_3(CO)_{12}]^- \rightarrow *[M_3(CO)_{12}]^- + 1e \rightleftarrows *[M_3(CO)_{12}]^{2-}$$

Noteworthy, in the case of $Ru_3(CO)_{12}$ reduction,[2b] Rieger and co-workers have speculated that the primary process, which the electrogenerated short-lived *triangulo*-$Ru_3(CO)_{12}$ undergoes, is ring opening to a *linear* $*[Ru_3(CO)_{12}]$ radical. This is in accord with the metal–metal antibonding character of the LUMO as previously discussed.[3]

Coordination of polydentate ligands to the metallic core claps several metal atoms together and usually increases the lifetime of the electrogenerated ionic species when compared with parent clusters. Examples for this are the electrochemical behavior of $FeCo_2(CO)_9(\mu_3\text{-}E)$ (E = S, Se, PR)[4] and $Co_3(CO)_9(\mu_3\text{-}CR)$[5] series. In principle, the coordination of large organic chains, interacting with the metallic frame in a multicentered σ/π fashion, results in increasing the electronic delocalization over the entire molecule and should further improve the stability of the corresponding ionic species. Indeed, we have recently reported that the $Fe_3(CO)_8(alkyne)_2$ clusters,[6] where an extensive electronic delocalization has been predicted by theoretical calculations,[7] show two subsequent, fully reversible reduction processes.

In order to compare this electrochemical behavior with that of homologous triruthenium derivatives, we have synthesized three $Ru_3(CO)_8(alkyne)_2$ derivatives and investigated their electrochemistry in nonaqueous solvents. Quantum mechanical calculations, within the Fenske–Hall scheme, and electronic spectra have been obtained and correlated with the formal electrode potentials.

Results and Discussion

Spectroscopic Characterization and Electrochemical Behavior. The $Ru_3(CO)_8(alkyne)_2$ compounds are isostructural with $Fe_3(CO)_8(PhC_2Ph)_2$[8] as clearly established by several X-ray structural determinations,[9] carried out during alkyne oligomerization studies. Their idealized C_{2v} structure is shown in Figure 1, along with the numbering scheme used in the text.

The homosubstituted alkyne clusters of the formula $Ru_3(CO)_8(RC_2R)_2$ (namely, **1**, R = Ph, and **2**, R = Et) have been synthesized by refluxing $Ru_3(CO)_{12}$ with an excess of the appropriate alkyne in toluene[10] (yields: **1**, ca. 40%; **2**, ca. 50%). The heterosubstituted alkyne cluster Ru_3-

(1) (a) Lemoine, P. *Coord. Chem. Rev.* **1988**, *83*, 169. (b) Geiger, W. E.; Connelly, N. G. *Adv. Organomet. Chem.* **1984**, *23*, 1; **1985**, *24*, 87.
(2) (a) Bond, A. M.; Dawson, P. A.; Peake, B. M.; Robinson, B. H.; Simpson, J. *Inorg. Chem.* **1977**, *16*, 2199. (b) Cyr, J. C.; DeGray, J. A.; Gosser, D. K.; Lee, E. S.; Rieger, P. H. *Organometallics* **1985**, *4*, 950. (c) Downard, A. J.; Robinson, B. H.; Simpson, J.; Bond, A. M. *J. Organomet. Chem.* **1987**, *320*, 363.
(3) Tyler, D. R.; Levenson, R. A.; Gray, H. B. *J. Am. Chem. Soc.* **1978**, *100*, 7888.
(4) Peake, B. M.; Rieger, P. H.; Robinson, B. H.; Simpson, J. *Inorg. Chem.* **1981**, *20*, 2540.
(5) Bond, A. M.; Peake, B. M.; Robinson, B. H.; Simpson, J. *Inorg. Chem.* **1977**, *16*, 410.
(6) Osella, D.; Arman, G.; Botta, M.; Gobetto, R.; Laschi, F.; Zanello, P. *Organometallics* **1989**, *8*, 620.
(7) (a) Casarin, M.; Ajò, D.; Granozzi, G.; Tondello, E.; Aime, S. *Inorg. Chem.* **1985**, *24*, 2141. (b) Thorn, D. L.; Hoffmann, R. *Nouv. J. Chim.* **1979**, *3*, 39.
(8) Dodge, R. P.; Schomaker, V. *J. Organomet. Chem.* **1965**, *3*, 274.
(9) Rosenberg, E.; Aime, S.; Milone, L.; Sappa, E.; Tiripicchio, A.; Lanfredi, A. M. M. *J. Chem. Soc., Dalton Trans.* **1981**, 2023 and references 7 and 8 therein.
(10) Cetini, G.; Gambino, O.; Sappa, E.; Valle, M. *J. Organomet. Chem.* **1969**, *17*, 437.

0276-7333/89/2308-2689$01.50/0

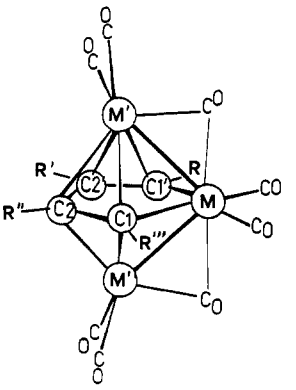

Figure 1. Idealized C_{2v} structure of $M_3(CO)_8(alkyne)_2$ compounds: M = Ru, R = R′ = R″ = R‴ = Ph, **1**; M = Ru, R = R′ = R″ = R‴ = Et, **2**; M = Ru, R = Me, R′ = Et, R″ = R‴ = Ph, **3**; M = Fe, R = R′ = R″ = R‴ = H, **4** (model compound); M = Ru, R = R′ = R″ = R‴ = H, **5** (model compound); M = Fe, R = R′ = R″ = R‴ = Ph, **6**; M = Fe, R = R′ = R″ = R‴ = Et, **7**; M = Fe, R = R′ = Et, R″ = R‴ = Ph, **8**.

Table I. IR, MS, and ^1H and ^{13}C NMR Data of the Following Compounds: $Ru_3(CO)_8(PhC_2Ph)_2$ (1), $Ru_3(CO)_8(EtC_2Et)_2$ (2), and $Ru_3(CO)_8(MeC_2Et)(PhC_2Ph)_2$ (3)

no.	IR $\bar{\nu}_{CO}$, cm^{-1} (*n*-hexane)	MS $[M]^+$,[a] *m/e*
1	2072 s, 2032 s, 2026 vs, 2018 s, 1978 s, 1880 m, 1860 m	886[b]
2	2062 s, 2024 s, 2021 vs, 2002 s, 1972 s, 1879 m, 1859 m	694[b]
3	2067 s, 2030 s, 2024 vs, 2010 s, 1975 s, 1878 m, 1856 m	776[b]
no.	^1H NMR δ, ppm ($CDCl_3$, recorded at 270 MHz)	
1	7.42 (m, 4, oPh_2), 7.15 (m, 6, m+pPh_2), 6.87 (m, 6, m + pPh_1), 6.24 (m, 4, oPh_1)	
2	3.06 [q, 4, $CH_2(Et_2)$], 1.62–1.46 [m, 5, $CH_2(Et_1)$ + $CH_3(Et_2)$], 0.51 [t, 3, $CH_3(Et_1)$]	
3	7.72 (m, 2, oPh_2), 7.39 (m, 3, m+pPh_2), 6.79 (m, 3, m+pPh_1), 6.12 (m, 2, oPh_1), 2.84 (s, 3, CH_3), 1.66 (m, 2, CH_2CH_3), 0.62 (t, 3, CH_2CH_3)	
no.	^{13}C NMR[c] δ, (ppm, $CDCl_3$, recorded at 67.9 MHz)	
1	144.1–126.7 (Ph), 124.6 (C_1), 117.6 (C_2)	
2	123.9 (C_1), 122.3 (C_2), 34.3 [$CH_2(Et_1)$], 24.7 [$CH_2(Et_2)$], 22.9 [$CH_3(Et_2)$], 20.4 [$CH_3(Et_2)$]	
3	144.3–126.5 (Ph), 126.3, 124.4, 116.4, 115.1 (C_{ac}), 35.5 (CH_2), 19.6 (CH_3), 18.4 (CH_2CH_3)	

[a] Calculated on ^{102}Ru. [b] Followed by stepwise loss of eight CO's. [c] Resonances of the organic chain only (sample not enriched in ^{13}CO).

$(CO)_8(MeC_2Et)(PhC_2Ph)$ (**3**) has been prepared through a two-step synthesis.[11] The stable $Ru_3(H)(CO)_9(MeC{\cdots}CH{\cdots}CMe)$ intermediate is firstly obtained by heating $Ru_3(CO)_{12}$ with 1,3-pentadiene in cyclohexane through the well-established oxidative-addition reaction. It is then purified and reacted further with excess of PhC_2Ph in refluxing *n*-heptane to give **3** in ca. 45% yield. Their purity has been checked by IR, NMR, and MS spectrometry (Table I).

The assignment of their NMR spectra has been achieved by two-dimensional and selective decoupling experiments and, as expected, is fully consistent with that of the homologous $Fe_3(CO)_8(alkyne)_2$ derivatives[6] (Table I). In particular, the C_1 substituents resonate at *higher* field with respect to the C_2 ones in the proton spectra. In contrast, C_1 substituents and C_1 atoms resonate at *lower* field with respect to C_2 substitutents and C_2 atoms themselves in the ^{13}C NMR spectra. This inverse trend can be ascribed to the anisotropic effect of the nonbonding electrons of the M′ transition-metal atoms, which predominates in the proton spectra.

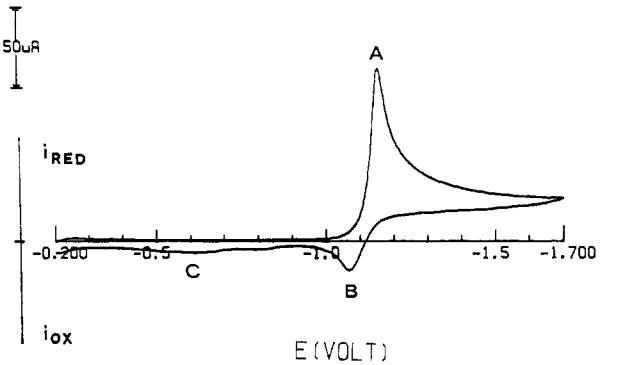

Figure 2. Cyclic voltammogram recorded at a mercury electrode on a CH_2Cl_2 solution containing 1 (1.0 mM) and $[NBu_4][ClO_4]$ (0.1 M) (room temperature (18 °C), scan rate = 200 mV s^{-1}).

In Figure 2 the cathodic part of the cyclic voltammogram exhibited by $Ru_3(CO)_8(PhC_2Ph)_2$ (**1**) in CH_2Cl_2 at room temperature (18 °C) is reported. A single reduction wave is observed (peak A at E_p = −1.16 V) coupled with the reoxidation response B in the reverse scan. It is evident from the peak current ratio, $i_p(B)/i_p(A)$, of about 0.4 at 200 mV s^{-1}, and from the minor oxidation peak C (at ca. −0.62 V) that fast chemical complications follow the reduction.

Controlled potential coulometry at E_w = −1.20 V and room temperature indicates that the overall reduction process consumes 2.5 faradays/mol of **1**.

Analysis of waves A and B at scan rate varying from 0.05 to 50 V s^{-1} (at 0.02 V s^{-1} the reoxidation peak is totally absent) indicates the following. The anodic to cathodic current ratio, $i_p(B)/i_p(A)$, increases from 0.22 to 1 (at 5.0 V s^{-1}); the current function, $i_p(A)/v^{1/2}$, which is proportional to $n_{app}^{3/2}$ (n_{app} = number of electrons transferred), decreases more then twice; the difference between the potential of the cathodic wave and that of its directly associated reoxidation one, $\Delta E_p = E_p(B) - E_p(A)$, gradually increases from 70 to 420 mV.

Furthermore, chronoamperometric experiments at E_w = −1.20 V and room temperature, employing periods (τ) ranging from 0.003 to 3 s, indicate that the $it^{1/2}$ term, which is proportional to n_{app}, remains constant within 3–600 ms, then progressively increases up to 1.4 times. All these data indicate that the overall reduction process is coupled with chemical reactions, which produce electroactive species even in the short time-window of cyclic voltammetric or chronoamperometric experiments.

Two resonable hypotheses can be advanced: (i) a quasi-reversible electron transfer process (E_{QR}) generates an unstable monoanion, which undergoes a fast chemical decomposition (C_{IRR}) to species in turn electroreducible at the working potential and then decomposable (an overall ECECE mechanism, which manifests the only ECE sequence in the time-window of cyclic voltammetry or chronoamperometry);[12] (ii) a quasi-reversible two-electron process [with $E^{\circ\prime}(1-/2-) \geq E^{\circ\prime}(0/1-)$]] generates an unstable dianion which rapidly decomposes to fragments that are themselves electroactive (an EECE mechanism).[12] Unfortunately, the number of electrons transferred (n_{app})

(11) (a) Aime, S.; Milone, L.; Osella, D.; Valle, M. *J. Chem. Res., Synop.* **1978**, 77; *J. Chem. Res., Miniprint* **1978**, 789–797. (b) Aime, S.; Osella, D.; Botta, M. *Organometallic Syntheses*; King, R. B.; Eisch, J. J., Eds.; Elsevier: New York, 1988, Vol. IV.

(12) (a) Bard, A. J.; Faulkner, L. L. *Electrochemical Methods*; Wiley: New York, 1980. (b) Brown, E. R.; Sandifer, J. R. *Physical Methods of Chemistry*; Rossiter, B. W., Hamilton, G. F., Eds.; Wiley: New York, 1986; Vol. II, Chapter IV.

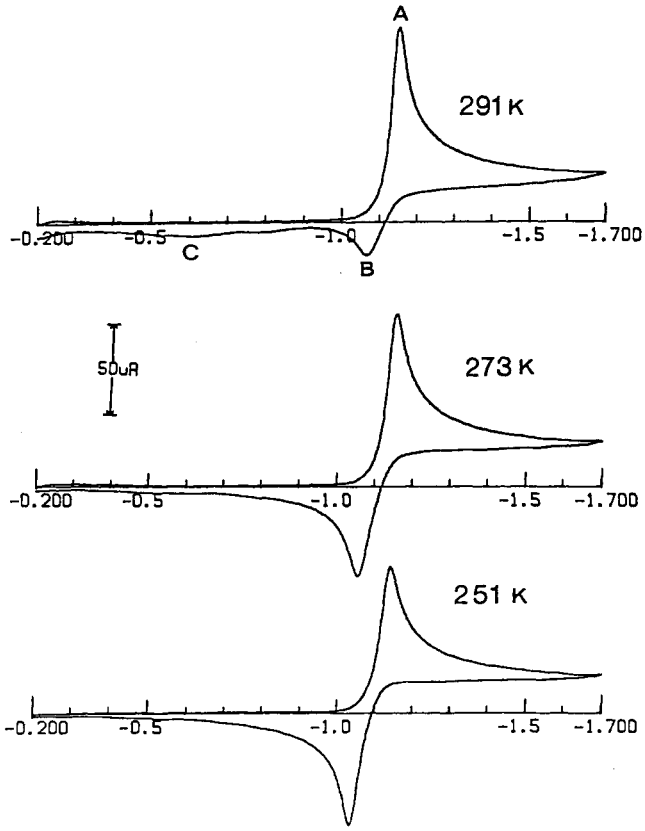

Figure 3. Cyclic voltammogram recorded at different temperatures on a dichloromethane solution of **1**. Experimental conditions are as in Figure 2.

cannot be simply deduced by the usual electrochemical criteria (i.e. ΔE_p for cyclic voltammetry or $[E_{3/4} - E_{1/4}]$ for polarography)[12] since the reduction process is not fully reversible.

A strong support to the ECECE mechanism comes from CV experiments at low temperature. The decrease of the temperature quenches the rate of the chemical reaction following the reduction step, and at −22 °C the CV response shows a $i_p(B)/i_p(A)$ ratio *equal* to unity and the full disappearance of peak C (Figure 3), indicating the complete chemical reversibility in the CV time scale. In addition, comparison of the reduction process with the one-electron oxidation of an equimolar amount of ferrocene [$FeCp_2$] at a platinum electrode shows that the peak current ratio $i_p^c(1)/i_p^a(FeCp_2)$ is 1.1 at +18 °C and becomes 0.7 at −22 °C. Provided that the decrease of the diffusion coefficient of **1** and $FeCp_2$ with the temperature is of the same magnitude, the neat decrease of the current ratio points to an ECE sequence. Macroelectrolysis of **1** at E_w = −1.20 V and at −22 °C is carried out until the current drops to 5%, of the initial value: at this point 1.0 ± 0.1 faraday/mol has been consumed.[13] The ESR spectrum of a dichloromethane solution of **1**, electrolyzed at E_w = −1.20 V and −30 °C up to 1 faraday/mol and then frozen at −173 °C, shows an axial structure ($g_\perp$ = 2.082, $g_\parallel$ = 2.010) very similar to that previously found[6] for the homologous monoanion $[Fe_3(CO)_8(PhC_2Ph)_2]^{\bullet-}$ (Figure 4). Noteworthy is the absence of any coupling with active ruthenium nuclei (i.e. ^{99}Ru and ^{101}Ru). The resolution of the ESR spectra at high gain is such that hyperfine couplings like those found for the reduction products of

(13) However, the current slowly flows beyond 2 electrons/molecule, suggesting that the chemical complications, even if slowed down, are still operative in the longer electrolysis time scale and generate electroactive fragments.

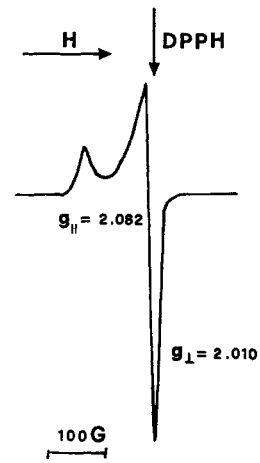

Figure 4. X-Band ESR spectrum of $[1]^{\bullet-}$ in CH_2Cl_2 frozen solution (100 K). DPPH (2,2′-diphenylpicrylhydrazyl) is employed as a reference.

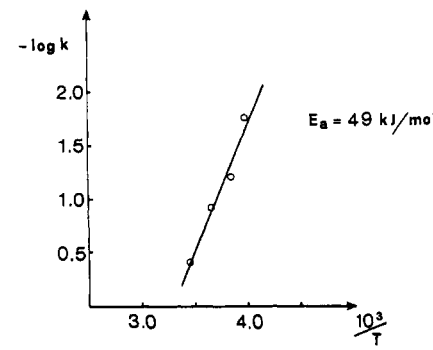

Figure 5. Arrhenius plot of the homogeneous chemical reaction following the reduction of **1**. The least-squares slope is 2.57 s^{-1} K and the correlation coefficient 0.967.

$Ru_3(CO)_{12}^{2b}$ should be discernible. This suggests a marked ligand character of the LUMO in accord with the results of the theoretical calculations (vide infra). This radical results to be stable only at the "glassy" state: as the temperature is increased up to the CH_2Cl_2 melting point, the signal rapidly vanishes.

CV tests with concentration of **1** ranging from 40 to 2 × 10^{-4} mol dm^{-3} reveal no substantial change in the response, indicating that a first-order reaction follows the reduction step. Making use of Nicholson–Shain's method,[14] a rate constant, k, can be evaluated at each temperature and then the activation energy, E_a, of the first homogeneous chemical reaction (ECECE) can be obtained (Figure 5). An attempt to clarify the overall electrochemical sequence leads to the following results. First, the exhaustive electrolysis of $Ru_3(CO)_8(PhC_2Ph)_2$ at E_w = −1.20 V and room temperature (2.5 electrons/molecule) followed by chemical reoxidation by air (O_2) gives *only* the binuclear $Ru_2(CO)_6(PhC_2Ph)_2$ complex, easily identified by IR (yield ca. 50%). Second, a sample of $Ru_2(CO)_6(PhC_2Ph)_2$, prepared according to the literature,[10] is irreversibly reduced at E_p = −1.84 V, well away from the working potential employed in the electrolysis of the parent compound. These data suggest that a solvated ruthenium carbonyl fragment, say "$Ru(CO)_2$", must be responsible for the excess of charge found in the coulometry experiments. Thus, we assign the reoxidation peak at −0.62 V, found in the room-temperature CV tests, to a species derived from "$Ru(CO)_2$". Interestingly a very similar E_p value has been found in the reoxidation scan of $Ru_3(CO)_{12}$.[2c]

(14) Nicholson, R. S.; Shain, I. *Anal. Chem.* **1964**, *36*, 706.

Table II. Redox Potentials (in V, vs SCE) for the Electron-Transfer Processes of Compounds 1–3 in CH_2Cl_2 or CH_3CN Solutions Containing $[Bu_4N][ClO_4]$ (0.1 M) Supporting Electrolyte

		0/1−			0/2+
no.	compd	$E^{o'}$, V CH_2Cl_2	E_p,[a] V CH_3CN	$t_{1/2}$ monoanion (s) at 18 °C (CH_2Cl_2)	E_p,[a] V CH_3CN
1	$Ru_3(CO)_8(PhC_2Ph)_2$	−1.16[b]	−1.00	0.7	+1.78
2	$Ru_3(CO)_8(EtC_2Et)_2$	−1.42[b]	−1.34	0.1	+1.33
3	$Ru_3(CO)_8(MeC_2Et)(PhC_2Ph)$	−1.28[b]	−1.18	0.3	+1.58

[a] Peak potential values at 0.2 V s^{-1} for irreversible processes. [b] Measured at scan rates for which $ip^{ox.}/ip^{red.}$ becomes equal to unity (1, 5 V s^{-1}; 2, 50 V s^{-1}; 3, 20 V s^{-1}).

Scheme I

$$Ru_3(CO)_8(PhC_2Ph)_2$$
$$\overset{+1e^-}{\underset{(E_{QR})}{\rightleftarrows}}$$
$$[Ru_3(CO)_8(PhC_2Ph)_2]^{\cdot-}$$
$$\downarrow (C_{IRR})$$
$$Ru_2(CO)_6(PhC_2Ph)_2 + \text{«}Ru(CO)_2\text{»}$$
$$\downarrow$$
$$(ECE\ldots)$$

Scheme I summarizes the overall mechanism. The stoichiometry of the above mechanism clearly indicates that CO should stabilize the highly unsaturated "$Ru(CO)_2$" fragment and then should increase the rate of the coupled chemical reaction. CV tests under N_2 and CO atmosphere confirm this hypothesis. The fragmentation rate of the monoanion $[Ru_3(CO)_8(PhC_2Ph)_2]^{\cdot-}$ is greatly enhanced by CO as testified by the disappearance of the reoxidation wave B and by the increase in peak C (Figure 6). The electrochemically induced transformation of $Ru_3(CO)_8(RC_2R)_2$ into $Ru_2(CO)_6(RC_2R)_2$ can be interpreted within the polyhedral skeletal electron pair (PSEP) approach[15] as a cluster contraction reaction from the closo ($S = 8$, $n = 7$) to the nido ($S = 8$, $n = 6$) pentagonal-bipyramidal geometry. Interestingly, Poe and co-workers have recently reported that $Os_3(CO)_9(\mu\text{-}C_4Ph_4)$ fragments to form $Os(CO)_5$ and $Os_2(CO)_6(C_4Ph_4)$ at rates proportional to CO concentration.[16]

In a coordinating solvent such as acetonitrile, the CV response of 1 is somewhat different. Even the use of high scan rate as well as the decrease of temperature are not able to support any pronounced reoxidation wave. Once again, this can be interpreted as the result of the stabilization of the unsaturated "$Ru(CO)_2$" fragment by solvation by CH_3CN molecules. Alternatively, the "$Ru(CO)_2$" species could be reacting with MeCN in the ETC reaction.[17] In turn, this increases the decomposition rate of the monoanion.

The voltammetric behavior is qualitatively common to all triruthenium derivatives 1–3 and the relevant redox potentials, both at mercury and platinum working electrodes, are summarized in Table II. In contrast to the triiron homologues, which undergo two distinct, irreversible one-electron oxidations,[6] the triruthenium derivatives show a single two-electron irreversible oxidation step.

Once again, the redox potentials are sensitive to the electronic properties of the substituents of the metallacycle, suggesting a high electronic delocalization in the cluster.[6]

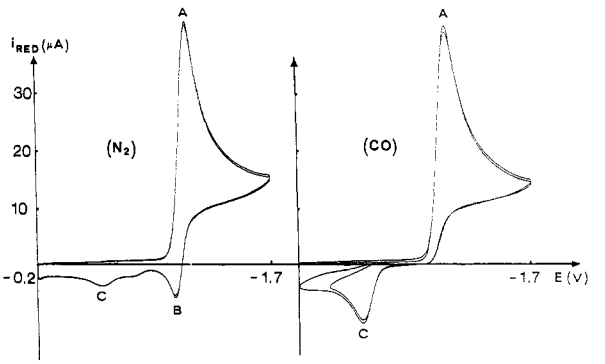

Figure 6. Cyclic voltammogram recorded at a Hg electrode on a CH_2Cl_2 solution of 1 under N_2 and CO (temperature = 18 °C; scan rate = 200 mV s^{-1}).

Theoretical Calculations. Fenske–Hall[18] calculations were carried out on the model compounds $Fe_3(CO)_8(HC_2H)_2$ (4) and $Ru_3(CO)_8(HC_2H)_2$ (5). Structural parameters were taken from the known compounds $Fe_3(CO)_8(PhC_2Ph)_2$[8] and $Ru_3(CO)_8(C_{12}H_{18})$,[9] although the model compounds were idealized to C_{2v} symmetry. A numbering scheme for 4 and 5 is given in Figure 1. The bonding in 4 and 5 has, in each case, been considered in terms of the interactions of the trimetal fragment $M_3(CO)_8$ and the butadiene fragment C_4H_4.

The observed changes in C–C bond lengths in going from free, molecular C_4H_6 to the complexed C_4H_4 unit in 4 or 5 are not included in the calculation. Any results quoted below for "free C_4H_4" refer to a fragment with a geometry taken from 4 or 5. Thus, any effects observed in going from free to coordinated C_4H_4 (e.g. C–C bond weakening) are caused by metal–ligand interactions and are not biased by a built-in change in bond length.

Interaction of the Fragments $M_3(CO)_8$ (M = Fe, Ru) and C_4H_4. The relative energies and orbital compositions of the frontier orbitals of the $Fe_3(CO)_8$ and $Ru_3(CO)_8$ fragments are shown in Figure 7. With the exception of some differences in the percentage contributions of M versus M′ in MO's 55, 52, and 49, corresponding MO's for the two fragments possess, not surprisingly, the same characteristics as one another. Hence, each of the $Fe_3(CO)_8$ and $Ru_3(CO)_8$ fragments is expected to interact with the C_4H_4 fragment in basically the same manner. Figure 8 shows an orbital correlation diagram for the formation of compound 4. A parallel diagram drawn for the formation of 5 exhibits a few differences from Figure 8 in terms of the origins of the MO's of the two complexes. Corresponding MO's are correlated in Figure 9.

In 4, each of the MO's 48–51 possesses both $Fe_3(CO)_8$ and C_4H_4 fragment character, with the interfragment interactions (56–8), (53–9), (54–10), and (52–11) (Figures 8

(15) For a recent discussion see: Mingos, D. M. P. *Acc. Chem. Res.* **1984**, *17*, 311.
(16) Poe, A. J.; Sampson, C. N.; Smith, R. T. *J. Am. Chem. Soc.* **1986**, *108*, 5459.
(17) Kochi, J. K. *J. Organomet. Chem.* **1986**, *300*, 139.
(18) (a) Hall, M. B.; Fenske, R. F. *Inorg. Chem.* **1972**, *11*, 768. (b) Kostic, N. M.; Fenske, R. F. *Organometallics* **1982**, *1*, 974.

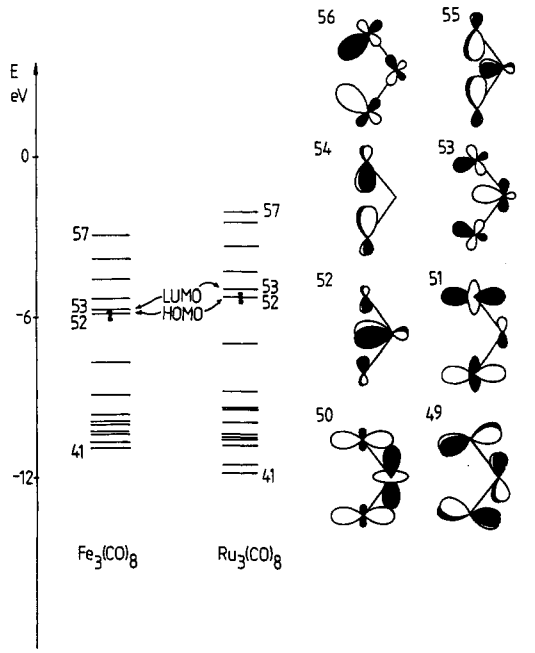

Figure 7. Relative energies and schematic representations of the frontier orbitals of the $Fe_3(CO)_8$ and $Ru_3(CO)_8$ fragments. Fragment orbital eigenvalues are taken from the Fock matrix of complexes **4** and **5**.

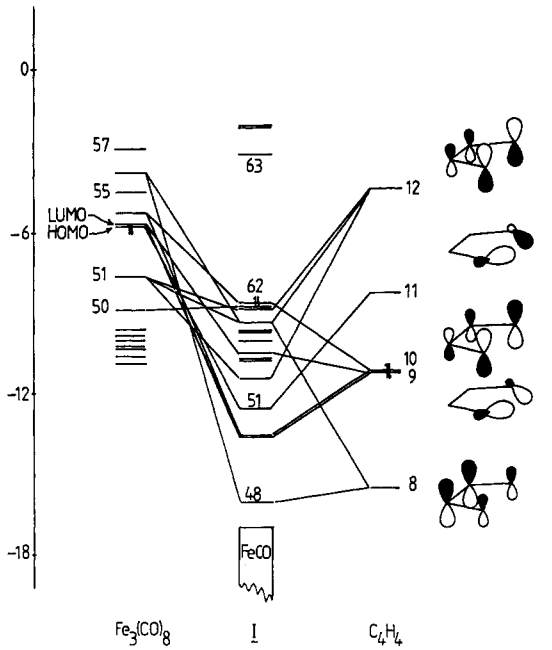

Figure 8. Orbital correlation diagram for the formation of **4** from $Fe_3(CO)_8$ and C_4H_4 fragments. Fragment orbital eigenvalues are taken from the Fock matrix of **4**.

and 10) being identified. The importance of these interactions may be assessed by considering the interfragment Mulliken overlap populations listed in Table III. The same observation is made with respect to the bonding in **5**. Note, however, that the complex MO corresponding to MO 51 in **4** is slightly destablized in going to **5** (Figure 9). This may be attributed to a change in the composition of the $M_3(CO)_8$ fragment MO 52 in going from M = Fe to M = Ru; for $Fe_3(CO)_8$, MO 52 exhibits 57% Fe and 9% each of Fe′ atoms, while in $Ru_3(CO)_8$, the corresponding orbital possesses 37% Ru and 19% each of Ru′ atoms. Thus, the direct overlap between atoms C(1) (or C(1′)) and Fe that results from the interaction of fragment MO's 52 and 11 (Figure 10) will be more effective in the case of the iron

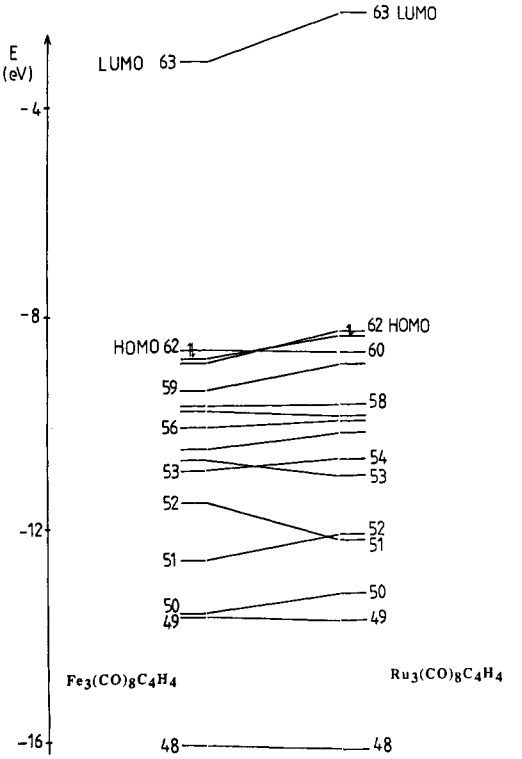

Figure 9. Comparison of the energies of and correlation of the orbitals of **4** and **5**.

Table III. Interfragment Mulliken Overlap Populations for the Interactions of $Fe_3(CO)_8$ with C_4H_4 To Form I and of $Ru_3(CO)_8$ and C_4H_4 To Form II[a]

MO in $M_3(CO)_8$ fragment	MO in C_4H_4					
	8	9	10 (HOMO)	11 (LUMO)	12	13
49			0.01 (0.01)			0.02 (0.01)
51					0.15 (0.16)	
52 (HOMO)				(0.26) (0.23)		
53 (LUMO)		0.24 (0.23)				
54			0.25 (0.24)			
55				... (0.04)		
56	0.14 (0.15)					

Total Interfragment Overlap Population = 1.07 (1.07)

[a] Populations for the formation of II are given in parentheses.

complex rather than the ruthenium complex. This is confirmed by the small decrease in Mulliken overlap population shown in Table III.

While exhibiting mostly metal character, MO's 62, 60, 59, 55, 54, and 52 of **4** do contain contributions from interfragment orbital combinations as shown in Figure 8. A similar pattern is noted for **5**. At this point, it is constructive to compare our results with those of Granozzi et al., obtained for complex **4** from a pseudopotential ab initio method.[7a] Qualitatively, the character of the MO's in **4** as determined by the Fenske–Hall approach appears similar to those described by Granozzi. The significant difference between the techniques is that in the Fenske–Hall method, lower energy MO's contain greater contributions of ligand character than do higher lying filled MO's, and interfragment interactions appear not to be as localized

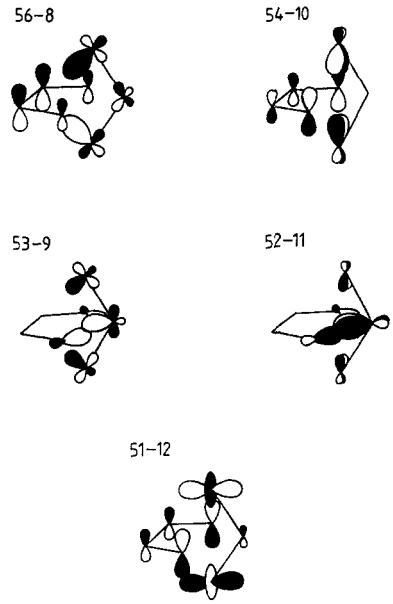

Figure 10. Schematic representations of the major interactions between the frontier orbitals of the fragments $M_3(CO)_8$ (M = Fe, Ru) and C_4H_4.

as has previously been suggested. For instance, the interaction (51–12), denoted by Granozzi as the Fe′→π_3* combination and localized in the SHOMO of $Fe_3(CO)_8C_4H_4$,[7a] appears, from our results, to be spread out over MO's 60, 59, 53, and 52 in **4** (or over MO's 62, 54, and 51 in **5**). Also significant, is the fact that the Fenske–Hall approach does not indicate the presence of large orbital contributions from the μ-CO ligands to the higher lying MO's of either **4** or **5**. This manifests itself most obviously in the description of the metal-based MO 61 in **4**. In agreement with the results of Granozzi, the $Fe_3(CO)_8$ fragment MO 50 does not interact with an orbital of the organic moiety. In our case, this fragment MO becomes MO 61 of both **4** and **5**, while appearing as the HOMO in the pseudopotential ab initio method. However, we again note negligible contributions from the μ-CO ligands, whereas the ab initio method indicates highly significant bridging carbonyl character.

Perturbation of the C_4H_4 Fragment upon Formation of 4 or 5. The interaction of fragment MO's 51 and 12 produces a transfer of electrons into a C_4H_4 fragment orbital which is C(1)–C(2) antibonding and C(2)–C(2′) π-bonding. The resultant effects of weakening C(1)–C(2) and strengthening C(2)–C(2′) are mirrored when MO 10 (HOMO) of the C_4H_4 fragment interacts with the vacant MO 54 of the $M_3(CO)_8$ framework. Electron density is transferred from ligand to metal; i.e., electrons are removed from an orbital which is C(1)–C(2) π-bonding and C(2)–C(2′) antibonding. However, there exists a competing effect that is brought about by the interaction of MO's 56 and 8. Here, transfer of electron density from the ligand to the metal results in a decrease in C(1)–C(2) and C(2)–C(2′) π-bonding. Together, these phenomena should manifest themselves in a shortening of the C(2)–C(2′) bond and a lengthening of the C(1)–C(2) bond as the organic moiety coordinates to the $M_3(CO)_8$ framework. Significantly, though, the results of the calculation suggest that the effect of weakening C(1)–C(2) should outweigh the strengthening of the C(2)–C(2′) bond.[19] Indeed, this is observed. In free butadiene, the carbon–carbon bond lengths are 1.35 (2) and 1.46 (3) Å,[20] whereas in $Fe_3(CO)_8(PhC_2Ph)_2$,[8] all the bonds are equal (1.45 (2) Å) within experimental error. This prompted Hoffmann to indicate these compounds as good candidates to show a six-π-electron aromaticity.[7b]

(19) Note that the results of the calculations are not biased by any built in change in C–C bond length upon complex formation.

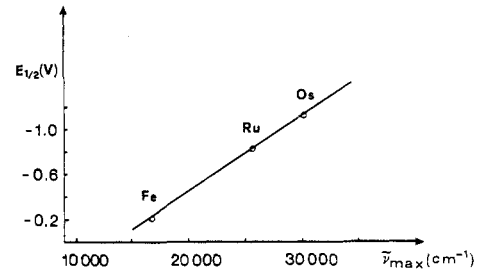

Figure 11. Plot of $E_{1/2}$ for the (0/1–) process[2] of $M_3(CO)_{12}$ (M = Fe, Ru, Os) clusters against the wavenumbers, $\bar{\nu}_{max}$, of their lowest energy electronic transitions[4] (in the $Os_3(CO)_{12}$ case, the shoulder at 385 nm has been ignored). The least-squares slope is −0.069 mV cm and the correlation coefficient 0.989.

HOMO – LUMO Separation in 4 and 5. Within the constraints of the Fenske–Hall quantum chemical approach, the HOMO – LUMO separations in **4** and **5** are 5.50 and 6.13 eV, respectively. The method tends to overestimate the energy of unoccupied MO's, and so it is the relative energies rather than the absolute values of these separations with which we should concern ourselves.

Final Remarks

In conclusion, while the $Fe_3(CO)_8(alkyne)_2$ series produces stable mono- and dianions on reduction, the ruthenium homologues give only quite unstable monoanions. This electrochemical behavior matches that of the parent clusters: the first reduction of $M_3(CO)_{12}$ (M = Fe, Ru, Os) becomes progressively more difficult as the atomic number of the metal atoms increases and the radical anion stability follows the order:[2]

$$Fe_3(CO)_{12} \gg Ru_3(CO)_{12} > Os_3(CO)_{12}$$

Electronic spectra indicate that the lowest energy dipole-allowed transition[3] (assumed to be metal–metal antibonding in character)[21] increases from $Fe_3(CO)_{12}$ to $Os_3(CO)_{12}$. As previously stated,[2a] a linear correlation can be obtained by plotting the one-electron half-wave potentials, $E_{1/2}$, against the wavenumbers, $\bar{\nu}_{max}$, of the visible bands, which represent the lowest energy gap (Figure 11). We have recorded the UV–vis spectra of compounds **1–3**, along with those of iron homologues, namely, $Fe_3(CO)_8(RC_2R)(R'C_2R')$ (R = R′ = Ph, **6**; R = R′ = Et, **7**; R = Et, R′ = Ph, **8**). Within the C_{2v} symmetry, the HOMO → LUMO excitation should be dipole-allowed and should correspond to the visible band. The Fenske–Hall quantum mechanical approach indicates an increasing HOMO – LUMO gap on passing from $Fe_3(CO)_8(HC_2H)_2$ to $Ru_3(CO)_8(HC_2H)_2$ model compounds, and, accordingly the triiron complexes are green while the triruthenium ones orange. A naive picture of the reduction process consists of one-electron transfer from the metal electrode Fermi level to the LUMO of the $M_3(CO)_8(alkyne)_2$ complex. Thus any increase of the HOMO – LUMO gap increases the $\bar{\nu}_{max}$ value and makes the reduction more difficult (in other words at more negative potentials). In more quantitative terms, two excellent linear correlations can be found by

(20) (a) Maris, D. J.; Sheppard, N.; Soicheff, B. P. *Tetrahedron* **1962**, *17*, 163. (b) Almenningen, A.; Bastiansen, O.; Traetteberg, M. *Acta Chem. Scand.* **1958**, *12*, 1221.

(21) Delley, B.; Manning, M. C.; Ellis, D. E.; Berkowitz, J.; Trogler, W. C. *Inorg. Chem.* **1982**, *21*, 2247.

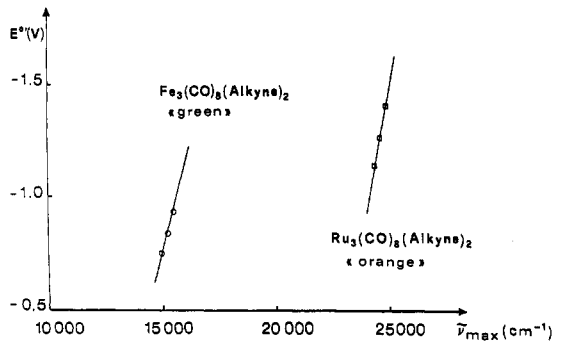

Figure 12. Plot of $E^{\circ\prime}$ for the (0/1−) process of $M_3(CO)_8(alkyne)_2$ (M = Fe, Ru) derivatives against the wavenumber, $\bar{\nu}_{max}$, of their visible bands. The slope for triiron clusters is −0.414 and that for triruthenium ones −0.446 mV cm. The correlation coefficients are 0.996 and 0.998, respectively.

plotting the formal electrode potentials, $E^{\circ\prime}(0/1-)$, against the wavenumbers, $\bar{\nu}_{max}$, for triiron and triruthenium derivatives, respectively (Figure 12). Noteworthy, the two straight lines are almost *parallel*, suggesting that the first reduction process (0/1−) is identical for both the series and simply for triruthenium compounds it occurs at higher energy.

Experimental Section

The $Ru_3(CO)_8(alkyne)_2$ compounds were synthesized according to the literature procedures,[10,11] as briefly described in the Results and Discussion.

The IR and MS spectra were recorded on a Perkin-Elmer 580 B and an AEI MS 12 instruments, respectively; the ^1H and ^{13}C NMR spectra on a JEOL GX-270-89 spectrometer. The ESR spectra were obtained from a Bruker 200 D-SRC instrument, operating at 9.78 GHz (X-band). The electronic spectra of ruthenium **1–3** and iron **6–8** derivatives were recorded in *n*-octane on a Varian Cary 219 spectrophotometer. The electrochemical apparatus was a BAS 100 A instrument. Purification procedures of solvents and supporting electrolytes have been described previously.[22] All potentials are referred to the saturated calomel electrode (SCE). Ferrocene was used as an internal standard. Under the actual experimental conditions the $FeCp_2^{0/1+}$ couple is located at +0.38 V in MeCN and +0.49 V in CH_2Cl_2.[23] The identification of $Ru_2(CO)_6(PhC_2Ph)_2$, the only product of the exhaustive electrolysis of **1**, was confirmed by TLC comparison with authentical sample.[10]

The Fenske–Hall calculations employed single-ξ Slater functions for the 1s and 2s functions of C and O. The exponents were obtained by curve fitting the double-ξ functions of Clementi[24] while orthogonal functions were maintained; the double-ξ functions were used directly for the 2p orbitals. An exponent of 1.16 was used for H. The Fe 1s–3d functions were from the results of Richardson[25] and were single-ξ, except for the 3d function which was double-ξ and chosen for the +1 oxidation state. Both 4s and 4p exponents for Fe were 2.00. Functions for Ru, chosen for the +1 oxidation state, were from the results of Richardson,[26] augmented by 5s and 5p functions with exponents of 2.20.

Acknowledgment. We gratefully thank the Italian MPI (Rome, Italy) and the European Economic Community (EEC) for financial support. The Royal Society is acknowledged for a 1983 University Research Fellowship (to C.L.H.) and the SERC for a grant (to S.M.O.). We thank P. A. Loveday (University Chemical Laboratory, Cambridge, U.K.) for high-pressure synthesis of $Ru_3(CO)_{12}$ and Johnson-Matthey Ltd. for a generous loan of $RuCl_3$.

Note Added in Proof. We are indebted to the reviewers for their invaluable suggestions.

Registry No. **1**, 94658-87-4; **2**, 95120-70-0; **3**, 68045-52-3; **4**, 119072-75-2; **5**, 122470-56-8; **6**, 12119-33-4; **7**, 94792-80-0; **8**, 94811-68-4; $Ru_3(CO)_{12}$, 15243-33-1.

(22) Bianchini, C.; Mealli, C.; Meli, A.; Sabat, M.; Zanello, P. *J. Am. Chem. Soc.* **1987**, *109*, 185.
(23) Gritzner, G.; Kuta, J. *Pure Appl. Chem.* **1982**, *54*, 1527.
(24) Clementi, E. *J. Chem. Phys.* **1964**, *40*, 1944.
(25) Richardson, J. W.; Nieuwpoort, W. C.; Powell, R. R.; Edgell, W. F. *J. Chem. Phys.* **1962**, *36*, 1057.
(26) Richardson, J. W.; Blackman, M. J.; Ranochak, J. F. *J. Chem. Phys.* **1973**, *58*, 3010.